Glucocorticoid receptor and RUNX transcription factors cooperatively drive CD8 T cells dysfunction in human cancer

Christopher J Ward[1$], Soura Chakraborty[1$], Sanu K Shaji[1], Clara Veiga-Villauriz[1], Qiuchen Zhao[1], Xi Chen[2] and Bidesh Mahata[1*]

1. Department of Pathology, University of Cambridge, Cambridge, CB2 1QP, UK

2. Shenzhen Key Laboratory of Gene Regulation and Systems Biology, Department of Biology, School of Life Sciences, Southern University of Science and Technology, Shenzhen, China

[$] Equal contribution

*To whom correspondence should be addressed: bm562@cam.ac.uk

Abstract

Glucocorticoids (GCs) are potent modulators of immune responses; however, the mechanisms by which GCs regulate gene expression in human CD8 T cells remain incompletely defined. Here, we delineate how physiological cortisol signalling shapes the transcriptional and chromatin landscapes of primary human CD8 T cells. We identify a substantial cohort of GC-responsive genes that are co-regulated through the cooperative activity of the glucocorticoid receptor (GR) and RUNX transcription factors. Integrative RNA sequencing and ChIP sequencing analyses identified genome-wide cortisol-responsive immunoregulatory genes. Genetic deletion of the glucocorticoid receptor (GR, encoded by *NR3C1*) abolished cortisol-induced gene expression changes, confirming GR-dependency. Notably, GR chromatin occupancy in cortisol-treated CD8 T cells was strongly enriched at RUNX transcription factor (TF) motifs rather than canonical glucocorticoid response elements (GREs). Co-immunoprecipitation assays validated a ligand-dependent physical interaction between GR and RUNX. Single-cell transcriptomic analyses of tumour infiltrating CD8 T cells revealed significant enrichment of cortisol-responsive genes, indicating an active GC signalling (response) within the tumour microenvironment. GR-RUNX dual controlled genes were enriched in tumour-infiltrating CD8 T cells across multiple cancer types, including lung adenocarcinoma, head and neck squamous carcinoma, pancreatic cancer, and breast cancer. We found GR-RUNX co-regulated genes are mostly expressed in the exhausted CD8 T cell population of different solid tumours These results suggest that local cortisol signalling within tumour microenvironments drives CD8 T cell dysfunction through GR-RUNX TF cooperation. Collectively, our findings identify RUNX TF as a critical mediator of GR signalling in human CD8 T cells and reveal a novel mechanism by which endogenous glucocorticoids influence antitumour immunity, which could be therapeutically targetable.

.

Introduction

Glucocorticoids (GCs) are steroid hormones widely recognised for their potent immunomodulatory and anti-inflammatory properties. Synthetic glucocorticoids, such as dexamethasone, betamethasone and prednisone, are extensively utilised in clinical settings to treat autoimmune disorders, inflammatory diseases, and haematological malignancies due to their ability to suppress immune cell activation and cytokine production[1,2]. Endogenous glucocorticoids, primarily cortisol in humans, also play critical roles in regulating immune homeostasis and responses under physiological and stress conditions[3]. Chronic or dysregulated GC signalling has been implicated in impaired antitumour immunity and cancer progression[2,4,5-7]. Despite extensive studies on synthetic GC-mediated immunosuppression, the precise molecular mechanisms by which physiological cortisol signalling modulates human CD8 T cell functions, particularly within tumour microenvironments, remain incompletely understood.

The glucocorticoid receptor (GR), encoded by the *NR3C1* gene, is a ligand-activated transcription factor belonging to the nuclear receptor superfamily. Upon ligand binding, GR translocate into the nucleus, binds chromatin at glucocorticoid response elements (GREs), and regulates target gene expression through direct DNA binding or tethering interactions with other transcription factors[8]. Although classical GRE-dependent mechanisms have been extensively characterised in various cell types, emerging evidence suggests that GR can also regulate gene expression through interactions with non-canonical transcriptional partners. GR can modulate gene expression in immune cells through protein–protein interactions with other transcription factors such as NF-κB and AP-1[9]. This “tethering” or “composite” model of gene regulation allows GR to repress or activate a distinct subset of genes indirectly, without binding DNA at traditional GRE motifs. For example, GR can bind to NF-κB p65 subunits, preventing NF-κB from inducing proinflammatory cytokine transcription. Conversely, it can cooperate with AP-1 to enhance the expression of anti-inflammatory mediators. Such interactions enable GR to modulate gene expression programs in a highly context-dependent manner[10,11]. Identification of these non-canonical GR partners in specific immune subsets is crucial for understanding the complex regulatory networks orchestrated by glucocorticoids in a physiological or pathological contexts of immune regulation.

CD8 T cells are central players in adaptive immunity, mediating cytotoxic responses against infected cells (such as virus infected) or cancer cells. Effective CD8 T cell responses are critical for tumour control and elimination. However, persistent antigen exposure and immunosuppressive signals within tumour microenvironments frequently drive CD8 T cell

dysfunction or exhaustion, limiting their antitumour efficacy[12,13]. In the context of CD8 T cells, GCs have been repeatedly shown to suppress T cell effector programmes, including the upregulation of checkpoint inhibitory proteins (CTLA-4, PD-1, LAG-3, TIM3) and the downregulation of co-stimulatory molecules (CD2, CD28 & 41BB) in a context dependent manner. Recent studies indicate that the local glucocorticoid signalling may contribute significantly to immune suppression within tumour microenvironment by promoting T cell dysfunction[2,4,5-7], yet the underlying transcriptional mechanisms remain largely unexplored.

RUNX transcription factors represent a family of evolutionarily conserved proteins crucially involved in lineage specification, differentiation, proliferation, and functional regulation of various immune cell subsets[14]. RUNX proteins (all three paralogues RUNX1-3) bind DNA through conserved Runt domains (>95% sequence identity) at core consensus motif YGYGGTY to regulate gene expression programs essential for hematopoietic development and immune function. Among the RUNX family members (RUNX1-3), RUNX2 is predominantly known for its roles in osteogenesis. However, recent evidence reveals its broader involvement in immune regulation and cancer biology[15]. RUNX1 and RUNX3 are critical regulators of CD8 T cell development and function. During thymopoiesis, they collaborate to repress CD4 and enforce CD8 lineage commitment[16,17]. In mature CD8 cytotoxic T lymphocytes (CTLs), RUNX3 dominates. It directly binds to the enhancers (e.g., *Cd8a* enhancer E8I) to maintain CD8 expression[16,17] and activating effector genes like *Ifng, Gzmb* (granzyme B), and *Prf1* (perforin) [16,17]. Runx3 deficiency severely impairs cytolytic activity and proliferation[16,17], while also promoting tissue-resident memory (T_{RM}) CD8 T cells by upregulating tissue-retention genes and suppressing recirculation[18]. Runx1 supports thymocyte transitions and mature T cell homeostasis but plays a secondary role in peripheral CTLs[19]. Runx2, though largely restricted to early thymic development, contributes to CD8 memory cell maintenance[1,18]. Together, Runx3 emerges as the central driver of CD8 T cell identity, effector function, and tissue residency, while Runx1 and Runx2 provide developmental and memory-related support. The potential interaction between GR signaling and RUNX transcription factors in CD8 T cells has not been previously investigated.

In this study, we aimed to elucidate how physiological cortisol signalling modulates human CD8 T cell function at the molecular level. Using integrative RNA sequencing (RNA-seq) and ChIP sequencing (ChIP-seq) approaches combined with genetic perturbations and biochemical validations, we demonstrate that cortisol profoundly reshapes the transcriptional landscape of primary human CD8 T cells through ligand-dependent GR-RUNX cooperation. We further provide single-cell transcriptomic evidence that this novel GR-RUNX regulatory axis operates within tumour-infiltrating CD8 T cells across multiple cancer types. Our findings

identify RUNX as a critical non-canonical partner of GR in human CD8 T cells and suggest a previously unrecognised mechanism by which local endogenous glucocorticoid signalling within tumour influence antitumour immunity, offering new therapeutic opportunities aimed at enhancing cancer immunotherapy efficacy by targeting context-specific GR interactions.

Results

Cortisol reshapes the transcriptional landscape and signalling pathways in human activated CD8 T cells

To investigate how physiological cortisol influences the transcriptional profile of human CD8 T cells, we performed RNA-seq on *in vitro* activated primary CD8 T cells treated with cortisol (100 nM, 48 hours) or vehicle control (Figure 1a). Differential gene expression analysis identified 332 significantly regulated genes (170 upregulated, 162 downregulated) (Figure 1b). Among the most strongly induced genes were *TSC22D3, IL7R, FKBP5 and PIK3IP1*. Notably, *PIK3IP,* a negative regulator of PI3Ks, *and* amphiregulin (*AREG*), a cytokine implicated in tissue repair and immunosuppression, emerged as a novel cortisol-induced gene in CD8 T cells. A complete list of these differentially expressed genes can be accessed in the Supplementary Table S1. Gene set enrichment analysis (GSEA) using the Hallmark gene set collection revealed distinct patterns of pathway regulation following glucocorticoid treatment (Figure 1c, Supplementary Table S2). Significantly upregulated pathways include E2F targets, MYC targets, G2M checkpoint, and mTORC1 signalling, indicating enhanced cell cycle regulation and metabolic reprogramming. Conversely, downregulated pathways comprise inflammatory response, TNFα signalling via NF-κB, IL6/JAK/STAT3 signalling, KRAS signalling (both up and down gene sets), apoptosis, and IL2/STAT5 signalling. These data suggest cortisol enforces a metabolic checkpoint state in CD8 T cells, limiting inflammatory effector functions while simultaneously promoting cell survival and proliferation-associated pathways.

To confirm GR-dependency of these transcriptional changes, we employed CRISPR-Cas9-mediated knockout of the glucocorticoid receptor gene (*NR3C1*) in primary human CD8 T cells (Fig 1d). Loss of GR expression abolished cortisol-induced upregulation of target genes (e.g., *TSC22D3*, *IL7R, FKBP5, PIK3IP1 and AREG*), confirming direct GR involvement in mediating cortisol-driven transcriptional reprogramming (Figure 1e). A complete list of differentially expressed genes in NR3C1 knocked out CD8 T cell can be found in Supplementary Table S1.

In CD8 T cells, these 123 genes get upregulated in hydrocortisone treatment but downregulated when the glucocorticoid receptor gene (*NR3C1*) is knocked out. The Venn

147 diagram analysis demonstrated that 47 genes were exclusively upregulated by cortisol in a
148 GR-independent manner (Mock HC vs. Veh), while 54 genes were uniquely upregulated in
149 GR-KO cells independent of the ligand cortisol (Figure 1f). 123 genes were commonly
150 upregulated in both conditions, suggesting GR-dependent mechanisms of cortisol-induced
151 gene activation. Similarly, we found 85 genes get downregulated in cortisol treated CD8 T cell
152 and get upregulated in *NR3C1* KO CD8 T cells. These findings identify cortisol induced true
153 upregulated and downregulated genes in CD8 T cells. These findings also indicate that while
154 a substantial proportion of cortisol-regulated genes require functional GR signalling, a subset
155 of genes are expressed in a cortisol or GR-independent mechanisms.
156
157 To gain further insight into the functional implications of cortisol-induced transcriptional
158 changes, we examined differentially expressed genes encoding transcription factors and
159 various receptors (Figure 1g). The heatmap analysis revealed distinct expression patterns of
160 transcription factors regulated by cortisol treatment in both GR-sufficient and GR-deficient
161 conditions. Several transcription factors, including *ZBTB16, ELK3, TSC22D3 and CEBPB*,
162 showed pronounced regulation following cortisol treatment. The receptor expression analysis
163 identified multiple classes of differentially expressed receptors, including cytokine receptors
164 (e.g., IL10RA, CCR7, IL7R, CXCR4), transporters (e.g., SLC3A2, SLC1A5), cell surface and
165 adhesion receptors (e.g., PTGIR, ITGB2, ADGRG5), and nuclear receptors VDR and
166 TSC22D3. Among these, several interleukin receptors showed predominantly GR-dependent
167 regulation, while others exhibited mixed patterns of GR-dependent and independent
168 expression changes. These findings highlight the complex interplay between GR-dependent
169 and independent mechanisms in mediating the effects of cortisol on the transcriptional
170 landscape of CD8 T cells, with potential implications for understanding glucocorticoid actions
171 on immune function.
172
173 Together, these results demonstrate that physiological cortisol reshapes the transcriptional
174 landscape of human CD8 T cells through GR-dependent regulation of immunomodulatory
175 genes and pathways, highlighting a novel role for glucocorticoids in controlling T cell
176 functionality via metabolic checkpoint enforcement.
177
178 **Genome-wide chromatin occupancy reveals the direct target genes of GR and its**
179 **noncanonical association with RUNX transcription factors**
180 To elucidate the molecular mechanisms underlying cortisol-mediated transcriptional
181 reprogramming in activated CD8 T cells, we performed chromatin immunoprecipitation
182 followed by sequencing (ChIP-seq) to map genome-wide glucocorticoid receptor (GR) binding
183 sites upon cortisol treatment. Primary human CD8 T cells from healthy donors were activated

184 *in vitro* and treated with cortisol (100 nM, 48 hours) or vehicle (Figure 2a). GR-bound
185 chromatin regions were identified by ChIP-seq. Cortisol treatment markedly increased GR
186 occupancy across the genome, identifying a total of 4871 high-confidence GR binding peaks
187 compared to vehicle-treated controls (Figure 2b, Supplementary Table S3). Motif enrichment
188 analysis of these GR-bound genomic regions surprisingly revealed no significant enrichment
189 of canonical glucocorticoid response elements (GREs), however, showed a striking
190 enrichment of non-canonical enrichment of RUNX transcription factor binding motifs upon
191 cortisol treatment (Figure 2b). Specifically, RUNX motifs were present in approximately 12.6%
192 of GR-bound peaks in cortisol-treated cells. Other transcription factor motifs such as TEAD
193 and NFAT also showed modest enrichment following cortisol stimulation (Figure 2b). These
194 data suggest that cortisol-induced GR chromatin occupancy in CD8 T cells preferentially
195 occurs at genomic loci harbouring non-canonical binding to other TFs sites, particularly RUNX
196 binding sites rather than canonical glucocorticoid response elements (GREs). In depth ChIP-
197 seq analysis of CD8 T cell identifies 1103 common peaks between two individual CD8 T cells
198 treated with hydrocortisone (Figure 2c), and 344 common peaks between vehicle-treated and
199 hydrocortisone treated CD8 T cell (Figure 2d). We found 81 direct targets of glucocorticoid by
200 integrating GR occupied genes (obtained from ChIP-seq) and glucocorticoid induced
201 upregulated genes (Figure 2e). We also observed out of 81 direct targets of GR 50 genes are
202 co-regulated by GR-RUNX (Figure 2f). Notably, genes exhibiting GR occupancy enriched with
203 RUNX motifs included critical immunoregulatory targets such as TSC22D3, IL7R, FKBP5,
204 PIK3IP1 and FAM53B, all significantly upregulated upon cortisol stimulation (Figure 2g).
205 Further genomic annotation analysis indicated that cortisol-induced GR binding predominantly
206 localised to intronic (31%) and promoter-proximal regions (31%), contrasting with classical
207 GRE-driven enhancer occupancy typically observed in other cellular contexts (Figure 2h).
208 ChIP-seq analysis also revealed the following genes that directly controlled by the GR binding
209 to the promoter or locus control region of the target genes. The list of GR direct target genes
210 can be found in Supplementary Table S4.
211
212 **Ligand-dependent interaction between GR and RUNX3 orchestrates cortisol-induced**
213 **gene regulation in CD8 T cells**
214 Given the prominent enrichment of RUNX motifs at GR-bound genomic regions (Figure 2), we
215 hypothesised that GR might physically interact with RUNX transcription factors in a ligand-
216 dependent manner. To test this hypothesis, first we compared the expression level of RUNX
217 transcription factor in CD8 T cells and found RUNX3 is predominantly expressed
218 (Supplementary Figure S1a). Next, we performed co-immunoprecipitation (co-IP) experiments
219 in HEK293T cells transiently expressing GR and RUNX3 in the presence or absence of cortisol
220 stimulation (100 nM, 36 hours). Immunoblot analysis demonstrated that RUNX3 robustly co-

221 precipitated with GR only upon cortisol treatment, confirming ligand-dependent formation of a
222 GR-RUNX2 protein complex (Figure 3a).
223
224 To assess the functional relevance of this interaction in primary human CD8 T cells, we
225 integrated our GR ChIP-seq, RNA-seq with previously publicly available RUNX target genes
226 datasets that were reported based on RUNX ChIP-seq and RNA-seq. First, we integrated
227 RUNX1 target genes and the genes that were cortisol responsive and enriched with RUNX 1
228 motif. Notably, 12 genes displayed robust cortisol-induced expression coupled with proximal
229 GR-RUNX motif occupancy, suggesting direct transcriptional co-regulation by GR and RUNX
230 TFs (Figure 3b). Heatmap view in the right-hand-side panel of Figure 3b shows their GC and
231 GR dependency. Next, we integrated RUNX2 target genes and distinguished the genes that
232 are upregulated (45 genes) or downregulated (7 genes) by the cortisol induced GR-RUNX
233 complex (Figure 3c, left panels). Heatmap (right panel) shows the expression of these genes
234 in different conditions. to show their dependence on GC and GR. We observed 45 genes co-
235 upregulated by GR-RUNX3 and 5 genes co-downregulated by GR-RUNX3 in CD8 T cells.
236 (Supplementary Figure 1b). All the gene names corresponding to this figure have been listed
237 in supplementary table S5.
238
239 Collectively, these results demonstrate that cortisol induces a physical and functional
240 cooperation between GR and RUNX3 in CD8 T cells. This ligand-dependent interaction
241 expands the regulatory repertoire of glucocorticoids beyond classical GRE-mediated
242 transcriptional control, highlighting a previously unrecognised molecular mechanism by which
243 endogenous glucocorticoids modulate human CD8 T cell function.
244
245 **GR-dependent cortisol-induced gene signature is enriched in tumour-infiltrating CD8 T**
246 **cells across multiple cancer types**
247 Given our findings that cortisol signalling profoundly reshapes the transcriptional landscape of
248 human CD8 T cells via GR-RUNX cooperation, we next explored whether this regulatory axis
249 is relevant in the tumour microenvironment (TME). To address this, we analysed publicly
250 available single-cell scRNA-seq datasets from tumour-infiltrating lymphocytes derived from
251 patients with breast cancer (Figure 4a), lung adenocarcinoma (Figure 4b), head and neck
252 squamous cell carcinoma (HNSCC) (Figure 4c) and pancreatic adenocarcinoma (Figure 4d).
253 We examined whether the cortisol-responsive gene signature identified in our primary human
254 CD8 T cell model (including key genes such as *TSC22D3, IL7R, FKBP5, PIK3IP1* and *AREG*)
255 was enriched within tumour-infiltrating CD8 T cells compared to matched tissue or peripheral
256 blood CD8 T cells. Strikingly, single-cell transcriptomic analyses revealed a consistent and
257 significant enrichment of cortisol-induced genes in tumour-infiltrating CD8 T cells across all

four cancer types examined (Figure 4a-d). Furthermore, tumour-infiltrating CD8 T cells consistently expressed elevated levels of GR (*NR3C1*) compared to circulating counterparts, suggesting enhanced sensitivity to local glucocorticoid signalling within the tumour microenvironment.

These observations indicate that endogenous glucocorticoid signalling actively operates within tumour microenvironments to modulate CD8 T cell function, potentially contributing to an immunosuppressive state that favours tumour immune evasion. Collectively, these findings underscore the clinical relevance of GR-mediated transcriptional regulation in shaping immune responses within tumours and highlight the potential therapeutic value of targeting GR to reinvigorate antitumour immunity.

Elevated expression of RUNX-GR co-regulated genes in tumour-infiltrating CD8 T cells across cancer types

We investigated the expression patterns and functional significance of RUNX-GR co-regulated genes in CD8 T cells across multiple cancer types. Single-cell transcriptomic profiling was performed on CD8 T cells isolated from tumours and matched adjacent normal tissue or blood in four major malignancies: triple-negative breast cancer (TNBC), lung cancer, head and neck squamous cell carcinoma (HNSC), and pancreatic ductal adenocarcinoma (PDAC) (Figure 5a-d). RUNX-GR co-regulated genes exhibited significantly elevated expression in tumour-infiltrating CD8 T cells compared to their non-tumour counterparts across all examined cancer types (Figure 5a-d). The dot plots display both the proportion of cells expressing these genes (represented by dot size) and the relative expression intensity (indicated by colour intensity), with both parameters markedly increased in tumour-infiltrating populations. Whilst we employed RUNX2-GR regulated genes for our analysis, it is important to note that this gene set encompasses RUNX1-GR regulated genes, effectively representing broader RUNX-GR regulation. This approach is substantiated by the established functional redundancy among RUNX1, RUNX2, and RUNX3, which share a common core DNA-binding motif and frequently regulate overlapping target genes.

To assess the functional relevance of this expression pattern, we calculated module scores using the AddModuleScore method for individual CD8 T cells (Figure 5e-g). Higher module scores, indicative of elevated RUNX-GR co-regulated gene expression, strongly correlated with increased expression of established T cell exhaustion markers. This correlation was consistent across TNBC (Figure 5e), lung cancer (Figure 5f), HNSC (Figure 5g) and PDAC (Figure 5h), highlighting a conserved link between RUNX-GR transcriptional activity and the exhausted phenotype in tumour-infiltrating CD8 T cells.

These findings indicate that RUNX-GR dependent gene regulation is particularly prominent within the tumour microenvironment, suggesting its potential role in shaping the phenotype of tumour-infiltrating CD8 T cells.

Single-cell trajectory analysis reveals an association between cortisol-responsive gene expression and CD8 T cell dysfunction in cancer

To investigate how cortisol signalling affects CD8 T cell differentiation within the tumour microenvironment, we performed single-cell trajectory inference analysis on CD8 T cells isolated from lung tumours and paired peripheral blood samples from patients with lung cancer. Using the Monocle algorithm, pseudo-temporal trajectories were constructed based on single-cell transcriptomic profiles (Supplementary Figure S2A). Cells expressing high levels of cortisol-responsive genes (TSC22D3, IL7R, FKBP5) were predominantly positioned along trajectory branches associated with progression towards terminal exhaustion or dysfunction, characterised by increased expression of inhibitory receptors, such as *PDCD1, CTLA4, HAVCR2, TIGIT, LAYN, and TOX* (Supplementary Figure S2B). In contrast, cells exhibiting lower cortisol-responsive gene signatures were primarily associated with early activation states. These results suggest that glucocorticoid signalling within the tumour microenvironment is activated shortly after CD8 T cells infiltrate the tumour, potentially driving them toward dysfunctional differentiation states.

Discussion

In this study, we reveal that physiological cortisol signalling fundamentally remodels the transcriptional and chromatin landscapes of human CD8 T cells through a previously unrecognised, ligand-dependent cooperation between the GR and RUNX transcription factors. By integrating RNA sequencing, ChIP sequencing, genetic perturbation, biochemical validation, and single-cell transcriptomic analyses of tumour-infiltrating lymphocytes, we identify a novel GR-RUNX regulatory axis that significantly modulates CD8 T cell function within the tumour microenvironment.

Our findings extend the current understanding of GR biology, demonstrating that GR can regulate gene expression via non-canonical interactions with RUNX transcription factors, rather than exclusively through classical glucocorticoid response elements (GREs). Traditionally, GR-mediated transcriptional regulation has been attributed to direct DNA binding at GREs or through tethered interactions with factors such as NF-κB and AP-1[1,8]. Here, we provide evidence that, in cortisol-treated human CD8 T cells, GR preferentially occupies genomic regions enriched for RUNX motifs. Co-immunoprecipitation experiments confirm a

direct, ligand-dependent interaction between GR and RUNX3, positioning RUNX3 as a critical non-canonical partner that enables GR to access distinct regulatory regions beyond those governed by classical GRE-driven mechanisms.

RUNX transcription factors are established regulators of immune cell differentiation and function[14]. Our data uncover an unexpected role for RUNX3 in human CD8 T cells as a pivotal mediator of cortisol-induced immunomodulation. Genetic ablation of GR expression abolishes cortisol-induced gene expression changes, confirming direct GR dependency. Moreover, cortisol-induced genes with proximal GR-RUNX motif occupancy include key immunoregulatory factors such as IL7R, FKBP5, TSC22D3, PIK3IP1 and AREG, implicating RUNX as a crucial determinant of glucocorticoid-driven immunomodulation.

A particularly intriguing observation from our study is the paradoxical regulation of signalling pathways by cortisol in CD8 T cells. Cortisol robustly suppressed inflammatory pathways (e.g., TNF-α/NF-κB and IL-2/STAT5 signalling) while simultaneously activating pathways associated with cell survival and proliferation (mTORC1 signalling, G2/M checkpoint). This dual regulatory pattern suggests that cortisol enforces a metabolic checkpoint state, limiting inflammatory effector functions while promoting cellular survival pathways. Such metabolic reprogramming may facilitate prolonged persistence of dysfunctional or exhausted T cells within tumours, thus contributing to impaired antitumour immunity.

Our findings reveal that RUNX-GR dependent gene regulation is particularly prominent within the tumour microenvironment across multiple cancer types. This tumour-specific upregulation suggests that local factors within the tumour might be driving this regulatory programme. One potential mechanism could involve local steroid biosynthesis within the tumour microenvironment inducing the glucocorticoid signalling pathway, which subsequently activates RUNX-GR-mediated transcriptional programs that influence the fate and function of tumour-infiltrating CD8 T cells. The co-regulation by RUNX factors and GR in tumour-infiltrating T cells is particularly intriguing given that both transcription factor families have been implicated in immune cell differentiation and function. RUNX family transcription factors are known to function redundantly, with RUNX1, RUNX2, and RUNX3 often binding to the same genomic sites and collaboratively regulating similar target genes. Similarly, GR has been shown to collaborate with pioneer factors and other transcription factors to regulate cell type-specific transcriptional programs. The observed correlation between RUNX-GR co-regulated gene expression and T cell exhaustion markers suggests that this transcriptional program may contribute to the development of the exhausted phenotype that characterises many tumour-infiltrating T cells. This finding provides new insights into the molecular mechanisms that may

underlie T cell dysfunction within the tumour microenvironment and identifies potential therapeutic targets for enhancing anti-tumour immunity. Indeed, recent studies have highlighted local GC production within tumours as an immunosuppressive mechanism exploited by cancer cells to evade immune surveillance[2,42,4,5-7,20-25]. Our results provide mechanistic insights into how this local steroid signalling axis may operate at the transcriptional level through GR-RUNX cooperation leading T cell dysfunction.

From a translational perspective, our findings suggest novel therapeutic opportunities aimed at improving cancer immunotherapy efficacy by targeting context-specific GR interactions. Systemic inhibition of glucocorticoid signalling is challenging due to adverse effects; thus, selective disruption of GR-RUNX3 interactions or downstream targets identified herein may represent promising therapeutic strategies to enhance antitumour immunity without broadly compromising physiological GC functions. Future studies should explore small-molecule inhibitors or targeted genetic approaches to specifically disrupt GR-RUNX3 interactions in preclinical tumour models.

In conclusion, our study identifies RUNX3 as a novel non-canonical partner of GR in human CD8 T cells and reveals a previously unrecognised mechanism by which endogenous glucocorticoids modulate antitumour immunity. Targeting context-specific transcription factor interactions represents an exciting new avenue for therapeutic intervention aimed at reversing steroid-driven immunosuppression within tumours.

Limitations of the study

Nevertheless, several questions remain unanswered: First, although we demonstrated robust ligand-dependent GR-RUNX3 interaction *in vitro* and identified direct target genes through integrative genomic analyses, further studies are required to clarify the precise molecular determinants mediating this interaction at endogenous loci and its functional outcome changing chromatin structure at the endogenous locus. Second, additional research is needed to delineate the relative contributions of RUNX family members in mediating GC responses in distinct immunological contexts. Finally, future work should validate our findings using *in vivo* tumour models to assess whether disrupting GR-RUNX interactions can effectively restore CD8 T cell functionality and enhance antitumour responses.

Methods

Human CD8 T cell culture

Peripheral blood samples were obtained from healthy male adult donors by informed consent. Peripheral blood mononuclear cells (PBMCs) were recovered through density gradient

406 centrifugation by Ficoll-Paque Plus (GE Healthcare). CD8 T cells were isolated from PBMCs
407 by immunomagnetic negative selection (Stem Cell Technologies). CD8 T cells were cultured
408 for a total of 8 days in Immunocult-XF T Cell Expansion media (Stem Cell Technologies) with
409 50 µg/mL of Gentamicin (Gibco). Isolated cells were stimulated with plate bound anti-CD3
410 (Biolegend, Clone: OKT3, 1 µg/mL) and anti-CD28 (Biolegend, Clone: CD28.2, 1 µg/mL) for
411 72 hours. Next, CD8 T Cells were rested and expanded in fresh Immunocult media in the
412 presence of 100 U/mL of human IL-2 (Peprotech) for a further 72 hours. Cells were then re-
413 stimulated with plate bound anti-CD3 (Biolegend, Clone: OKT3 1 µg/mL) and anti-CD28
414 (Biolegend Clone: CD28.2 1 µg/mL) in the presence of 100 nM of cortisol [hydrocortisone (HC)
415 – Sigma] or vehicle control (methanol, Sigma) for 48 hours.
416
417 **CRISPR-Cas9 mediated *NR3C1* deletion**
418 Seventy-two hours after T cell activation, cells were washed with PBS and resuspended in
419 complete P3 Primary Cell Nucleofection Solution (Lonza) according to the manufacturer's
420 instructions. For each nucleofection, 1×10^6 cells were used. Two distinct ribonucleoprotein
421 (RNP) complexes were prepared, each targeting a specific sgRNA designed for the deletion
422 of NR3C1. The sequences for the sgRNAs were as follows:
423 1. sgRNA 1: 5' – CUUUAAGUCUGUUUCCCCCG – 3'
424 2. sgRNA 2: 5'– AACCUCCAACAGUGACACCA – 3'
425 Both sgRNAs were synthesised by Synthego, and the Alt-R S.p. High Fidelity Cas9 Nuclease
426 V3 (Integrated DNA Technologies) was used to form the RNP complexes. Each RNP complex
427 was assembled at a 3:1 molar ratio of sgRNA to Cas9 (2.48 µM Cas9 + 7.52 µM sgRNA). The
428 prepared Cas9 RNP complexes were mixed with the cells and transferred to a 20 µL
429 Nucleocuvette Vessel. Electroporation was performed using a 4D Nucleofector with the EO-
430 115 program (Lonza). For control experiments, NR3C1-sufficient CD8 T cells were processed
431 in parallel and electroporated with High Fidelity Cas9 protein only (Mock Control). Immediately
432 following nucleofection, 80 µL of pre-warmed ImmunoCult-XF media (without supplements)
433 was added directly to the Nucleocuvette Vessel, and the cells were allowed to recover at 37°C
434 for 20 minutes. The cells were then transferred to a 24-well plate and cultured for 72 hours in
435 fresh ImmunoCult-XF media supplemented with 100 U/mL of IL-2 (PeproTech) and 50 µg/mL
436 of Gentamicin (Gibco™).
437
438 **Single-cell RNA sequencing (scRNA-seq), clustering and visualisation**
439 The previously published and publicly available scRNA-seq datasets used in this study were
440 as follows GSE164690[26-28], GSE161529[29,30], GSE127465[31], GSE155698[32,33]. The data has
441 been downloaded from NCBI GEO (https://www.ncbi.nlm.nih.gov/geo/) and processed with
442 the standard scRNA-seq integration pipeline in Seurat. To cluster the cells, we first identified

443 the top 2,000 most variable genes using the FindVariableFeatures function in Seurat. For cell
444 visualization, we applied the Uniform Manifold Approximation and Projection (UMAP)
445 algorithm to project the cells' PCA space representation into two dimensions. Cell clustering
446 in PCA space was performed with the Shared Nearest Neighbor (SNN) algorithm, using
447 Seurat V3's FindNeighbors and FindClusters functions. We then visualised the resulting
448 clusters in UMAP space with the DimPlot function. The differentially expressed genes in each
449 cluster were identified with the FindAllMarkers function in Seurat. The clusters have been
450 identified either by previous annotation or based on the Cluster Identity Predictor (CIPR)
451 program and has been validated based on marker gene expression from Panglo DB. Gene
452 expression levels were visualised using heatmaps, violin plots, and bar plots, created with the
453 pheatmap package (version 1.0.12) (available at https://cran.r-
454 project.org/web/packages/pheatmap) and the dittoSeq R package (version 1.2.4). Data
455 scaling during visualization was performed automatically using the default settings of these
456 packages. Cell type information was retrieved from the meta.data slot of the downloaded
457 object. Gene module scores for subpopulations, as defined above, were calculated using the
458 Seurat function AddModuleScore.
459
460 **Single-cell trajectory analysis**
461 Single-cell trajectory analysis was performed using Monocle (version 2.20.0). Briefly, size
462 factors and dispersions were estimated with default settings. Differentially expressed genes
463 were identified using Monocle's differentialGeneTest function (q-value < 0.01). Identified
464 genes were used as ordering genes. Dimensionality was reduced using the DDRTree
465 algorithm, and trajectories were constructed by ordering cells based on pseudotime.
466
467 **Western blot analysis**
468 72 hours post nucleofection, CD8 T cells were washed once with ice cold PBS and lysed in
469 radioimmunoprecipitation assay (RIPA) buffer (Merck) with proteinase and phosphatase
470 inhibitors (Roche). Protein concentrations were determined by Pierce™ BCA Protein Assay
471 Kit and performed according to the manufacturer's instructions (Thermo-Scientific). Protein
472 samples (15 µg) were separated on a NuPAGE 4-12% Bis-Tris polyacrylamide gels
473 (Invitrogen), transferred onto nitrocellulose membranes (Bio-Rad) and probed using rabbit
474 anti-GR (Clone: D6H2L, Cell Signaling Technology) and mouse beta-actin (Clone: 8H10,
475 Origene) antibodies. Detection of immunoreactive bands was performed using secondary goat
476 anti-rabbit IRDye™ 680CW and goat anti-mouse IRDye™ 800CW antibodies and images
477 acquired on the Odyssey DLx imaging system (Li-COR).
478
479

480 **Bulk RNA sequencing analysis**

481 Cell pellets were layered with 40 µL of RNAlater Stabilization solution (Invitrogen) and stored
482 at -80°C prior to RNA extraction. Samples were homogenised using the QIAshredder Kit
483 (Qiagen) according to manufacturer's instructions. Next, total RNA was extracted using the
484 RNeasy Plus Mini Kit (Qiagen). RNA sequencing was performed in paired-end on a NextSeq
485 500 (Illumina) (HiSeq1500) platform, yielding 40 million reads per sample (Novogene, UK).
486 Raw sequencing reads were quality-controlled with FastQC (version 0.11.9), followed by
487 alignment to the reference genome gencode version 42 (Homo sapiens genome
488 hg38/GRCh38) using the alignment tool hisat2 (version 2.2.1). The sam files were further
489 inspected, filtered, and processed using samtools (version 1.13). HTseq counts obtained from
490 bam files were annotated and subjected to DESeq2 (version 1.34.0) analysis in R (version
491 4.1.1).. For DEseq2 analysis, for each gene, a log2 fold change was computed and the
492 significance level was assessed using the Wald test statistic with a p value and an adjusted p
493 value. Differentially expressed genes across different conditions have been identified using
494 the cutoff of a p-adjusted value of 0.05. The volcano plot has been constructed in GraphPad
495 Prism 9.5.1 based on the differentially expressed genes found in bulk RNA sequencing. After
496 differential expression analysis, genes were ranked according to their fold change and by
497 using the fGSEA algorithm, we performed Gene Set Enrichment Analysis (GSEA). The human
498 collection H (hallmark gene sets) from the Molecular Signatures Database (MSigDB) were
499 used to identify positively and negatively enriched pathways. All steps were performed in R
500 version 4.1.1.

501

502 **Chromatin immunoprecipitation (ChIP) followed by sequencing**

503 Chromatin immunoprecipitation (ChIP) was performed using the SimpleChIP Enzymatic
504 Chromatin IP Kit (Cell Signaling Technology) following the manufacturer's protocol with minor
505 modifications. Briefly, cells were crosslinked with 1% formaldehyde (Merck) in serum-free
506 RPMI-1640 for 10 min at room temperature (RT) and quenched with 1X glycine for 5 min.
507 Nuclei were isolated and chromatin digested with 0.3 µL micrococcal nuclease in 200 µL ChIP
508 Buffer at 37 °C for 20 min, followed by brief sonication (Branson 450-D sonicator, amplitude
509 36%, 4 × 5 s pulses on ice). Chromatin was immunoprecipitated overnight at 4 °C with 1 µg
510 each of anti-GR antibodies (PA1-511A, Thermo-Scientific; D6H2L, Cell Signaling
511 Technology). Immune complexes were captured with ChIP-Grade Protein G Magnetic Beads
512 (2 h, 4 °C), washed sequentially with low-salt and high-salt buffers, and eluted with 1X ChIP
513 Elution Buffer at 65 °C for 30 min. Crosslinks were reversed at 65 °C for 2 hours (5 M NaCl,
514 Proteinase K), with DNA purified and submitted for Illumina sequencing (Novogene,
515 Cambridge, UK).

516

517 **ChIP-seq data analysis**

518 Raw reads from fastq files were first trimmed using fastp 0.20.0 with the setting '-l 25 --
519 detect_adapter_for_pe'. Trimmed reads were mapped to the human genome hg38 by hisat2
520 2.1.0 with default setting and sorted by samtools 1.9 with flag '-ShuF 4 -q 30 -f 2'. After
521 mapping, duplicated reads were removed by the picard tool (v.2.20.8)
522 (http://broadinstitute.github.io/picard/). Peaks were then called using MACS2 and annotated
523 using HOMER.

524

525 **Integration of bulk RNA-seq and ChIP-seq data**

526 After analysing bulk RNA-Seq and ChIP-Seq data, we compared the differentially expressed
527 genes in RNA-seq of cortisol treated vs. vehicle control and all annotated peaks in ChIP-seq
528 data. Downstream analysis was performed based on the genes between the RNA-seq and
529 HC-treated ChIP-seq peaks, which include a total of 35 genes. The venn diagram to visualise
530 the common genes was constructed using InteractiVenn. A heatmap has been drawn in gplots
531 (version 3.1.3) in R version 4.1.1 to show the normalised counts of genes (transformed into
532 row z-score) common in differentially expressed genes in RNA-seq and annotated peaks from
533 cortisol (HC) treated cells. The protein-protein interaction (PPI) network has been constructed
534 in STRING (version 11.5) and visualised in cytoscape (version 3.91). All 35 differentially
535 expressed genes have been used as inputs in STRING, but only 8 genes constitute an intact
536 network. The pie chart demonstrating the genomic position diversity of peaks obtained from
537 cortisol treated cells in ChIP-seq data has been constructed in GraphPad Prism 9.5.1.

538

539 **Overexpression of NR3C1 and RUNX3 in HEK-293T**

540 A custom polycistronic plasmid (EF1A > hRUNX3 [NM_001320672.1] : IRES : hNR3C1
541 [NM_001364185.1] : IRES : EGFP) was designed and generated by VectorBuilder. Driven by
542 the EF1A promoter, this construct produces a single mRNA transcript translated into RUNX3,
543 NR3C1 (glucocorticoid receptor), and EGFP via IRES elements. HEK-293T cells were
544 transfected with 5 µg of plasmid using Lipofectamine 3000 (Invitrogen) in serum-free Opti-
545 MEM, following the manufacturer's protocol. Transfection was performed at 70–80%
546 confluence. After 6 hours, 100nM of cortisol (Sigma-Aldrich) was added directly to the culture
547 medium, and cells were incubated for an additional 48 hours to allow for cortisol-mediated
548 effects.

549

550 **Co-Immunoprecipitation (Co-IP)**

551 Cells were harvested by washing with ice-cold PBS and collected by centrifugation at 300 × g
552 for 5 minutes at 4 °C. Cell lysis was performed using Pierce IP Lysis Buffer (Thermo Scientific)
553 supplemented with protease and PhosSTOP phosphatase inhibitors (Roche). Lysates were

554 incubated on ice for 30 minutes, followed by mild sonication (three 5 s pulses at 36%
555 amplitude) using a Branson 4D Sonicator. Lysates were cleared by centrifugation at
556 16,000 × g for 20 minutes at 4 °C. The supernatant was pre-cleared by incubation with 10 µL
557 of Protein A/G Plus-Agarose Beads (Santa Cruz) for 1 hour at 4 °C with rotation, followed by
558 centrifugation at 3,000 × g for 10 minutes. Clarified lysates were incubated overnight at 4 °C
559 with either anti-NR3C1 (D6H2L, Cell Signaling Technology; 1:100) or control rabbit IgG (Cell
560 Signaling Technology), followed by addition of 30 µL Protein A/G Plus-Agarose Beads and
561 further incubation for 2 hours at 4 °C. Beads were washed three times with lysis buffer, and
562 bound proteins were eluted in Laemmli sample buffer. Eluates were analysed by western
563 blotting using anti-RUNX1/AML1, RUNX3, and RUNX2 antibodies (EPR3099, Abcam).
564

565 **Resource availability**

566 **Lead contact**

567 Further information and requests for resources and reagents should be directed to and will be
568 fulfilled by the Lead Contact, Bidesh Mahata (bm562@cam.ac.uk)

569 **Material availability**

570 This study did not generate unique reagents.

571 **Data and code availability**

572 - Data: All large datasets (RNA-seq and ChIP-seq) generated in this study will be
573 submitted to public repository.
574 - Code: This paper does not report original code.
575 - Additional information: Any additional information required to reanalyse the data
576 reported in this paper is available from the lead contact upon request.
577

578 **Author contribution**

579 CJW, SC, SKS, CVV, QZ and XC, performed the experiments, analysed, interpreted &
580 visualised the data. BM conceptualised and supervised the study. All authors read and
581 approved the draft manuscript before submission.
582

583 **Acknowledgements**

584 We would like to thank Amit Mandal, University of Oxford, for critical suggestion and advice
585 on RNA-seq data analysis. We used BioRender.com to generate the graphical illustrations
586 presented in this manuscript.

587

588

Funding

The work is supported by CRUK Career Development Fellowship (RCCFEL\100095), NSF-BIO/UKRI-BBSRC project grant (BB/V006126/1) and MRC project grant (MR/V028995/1).

Competing interests

The authors declare that they have no competing interests.

Data and materials availability

All newly generated data such as RNA sequencing and ChIP sequencing data used in the study will be available in the public database during revised submission stage.

Supplementary tables

Supplementary Table S1: Cortisol-induced genes in human CD8 T cell

Supplementary Table S2: Cortisol-induced hallmark pathways in CD8 T cell

Supplementary Table S3: Glucocorticoid binding peaks in CD8 T cell

Supplementary Table S4: Glucocorticoid direct target genes in CD8 T cell

Supplementary Table S5: Cortisol induced genes, ChIP-seq peaks, RUNX regulated genes

References

1. Cain, D.W., and Cidlowski, J.A. (2017). Immune regulation by glucocorticoids. Nat Rev Immunol *17*, 233-247. 10.1038/nri.2017.1.
2. Vandewalle, J., Luypaert, A., De Bosscher, K., and Libert, C. (2018). Therapeutic Mechanisms of Glucocorticoids. Trends Endocrinol Metab *29*, 42-54. 10.1016/j.tem.2017.10.010.
3. Quatrini, L., and Ugolini, S. (2021). New insights into the cell- and tissue-specificity of glucocorticoid actions. Cell Mol Immunol *18*, 269-278. 10.1038/s41423-020-00526-2.
4. Obradovic, M.M.S., Hamelin, B., Manevski, N., Couto, J.P., Sethi, A., Coissieux, M.M., Munst, S., Okamoto, R., Kohler, H., Schmidt, A., and Bentires-Alj, M. (2019). Glucocorticoids promote breast cancer metastasis. Nature *567*, 540-544. 10.1038/s41586-019-1019-4.
5. Acharya, N., Madi, A., Zhang, H., Klapholz, M., Escobar, G., Dulberg, S., Christian, E., Ferreira, M., Dixon, K.O., Fell, G., et al. (2020). Endogenous Glucocorticoid Signaling Regulates CD8(+) T Cell Differentiation and Development of Dysfunction in the Tumor Microenvironment. Immunity *53*, 658-671 e656. 10.1016/j.immuni.2020.08.005.
6. Mahata, B., Pramanik, J., van der Weyden, L., Polanski, K., Kar, G., Riedel, A., Chen, X., Fonseca, N.A., Kundu, K., Campos, L.S., et al. (2020). Tumors induce de novo steroid biosynthesis in T cells to evade immunity. Nat Commun *11*, 3588. 10.1038/s41467-020-17339-6.

628 7. Chakraborty, S., Pramanik, J., and Mahata, B. (2021). Revisiting steroidogenesis and its
629 role in immune regulation with the advanced tools and technologies. Genes Immun
630 *22*, 125-140. 10.1038/s41435-021-00139-3.
631 8. Weikum, E.R., Knuesel, M.T., Ortlund, E.A., and Yamamoto, K.R. (2017). Glucocorticoid
632 receptor control of transcription: precision and plasticity via allostery. Nat Rev Mol
633 Cell Biol *18*, 159-174. 10.1038/nrm.2016.152.
634 9. De Bosscher, K., Beck, I.M., Dejager, L., Bougarne, N., Gaigneaux, A., Chateauvieux, S.,
635 Ratman, D., Bracke, M., Tavernier, J., Vanden Berghe, W., et al. (2014). Selective
636 modulation of the glucocorticoid receptor can distinguish between transrepression of
637 NF-kappaB and AP-1. Cell Mol Life Sci *71*, 143-163. 10.1007/s00018-013-1367-4.
638 10. Escoter-Torres, L., Greulich, F., Quagliarini, F., Wierer, M., and Uhlenhaut, N.H. (2020).
639 Anti-inflammatory functions of the glucocorticoid receptor require DNA binding.
640 Nucleic Acids Res *48*, 8393-8407. 10.1093/nar/gkaa565.
641 11. Franco, L.M., Gadkari, M., Howe, K.N., Sun, J., Kardava, L., Kumar, P., Kumari, S., Hu,
642 Z., Fraser, I.D.C., Moir, S., et al. (2019). Immune regulation by glucocorticoids can be
643 linked to cell type-dependent transcriptional responses. J Exp Med *216*, 384-406.
644 10.1084/jem.20180595.
645 12. Wherry, E.J., and Kurachi, M. (2015). Molecular and cellular insights into T cell
646 exhaustion. Nat Rev Immunol *15*, 486-499. 10.1038/nri3862.
647 13. Philip, M., and Schietinger, A. (2022). CD8(+) T cell differentiation and dysfunction in
648 cancer. Nat Rev Immunol *22*, 209-223. 10.1038/s41577-021-00574-3.
649 14. Seo, W., and Taniuchi, I. (2020). The Roles of RUNX Family Proteins in Development of
650 Immune Cells. Mol Cells *43*, 107-113. 10.14348/molcells.2019.0291.
651 15. Mevel, R., Draper, J.E., Lie, A.L.M., Kouskoff, V., and Lacaud, G. (2019). RUNX
652 transcription factors: orchestrators of development. Development *146*.
653 10.1242/dev.148296.
654 16. Korinfskaya, S., Parameswaran, S., Weirauch, M.T., and Barski, A. (2021). Runx
655 Transcription Factors in T Cells-What Is Beyond Thymic Development? Front Immunol
656 *12*, 701924. 10.3389/fimmu.2021.701924.
657 17. Woolf, E., Xiao, C., Fainaru, O., Lotem, J., Rosen, D., Negreanu, V., Bernstein, Y.,
658 Goldenberg, D., Brenner, O., Berke, G., et al. (2003). Runx3 and Runx1 are required for
659 CD8 T cell development during thymopoiesis. Proc Natl Acad Sci U S A *100*, 7731-7736.
660 10.1073/pnas.1232420100.
661 18. Milner, J.J., Toma, C., Yu, B., Zhang, K., Omilusik, K., Phan, A.T., Wang, D., Getzler, A.J.,
662 Nguyen, T., Crotty, S., et al. (2017). Runx3 programs CD8(+) T cell residency in non-
663 lymphoid tissues and tumours. Nature *552*, 253-257. 10.1038/nature24993.
664 19. Egawa, T., Tillman, R.E., Naoe, Y., Taniuchi, I., and Littman, D.R. (2007). The role of the
665 Runx transcription factors in thymocyte differentiation and in homeostasis of naive T
666 cells. J Exp Med *204*, 1945-1957. 10.1084/jem.20070133.
667 20. Taves, M.D., Otsuka, S., Taylor, M.A., Donahue, K.M., Meyer, T.J., Cam, M.C., and
668 Ashwell, J.D. (2023). Tumors produce glucocorticoids by metabolite recycling, not
669 synthesis, and activate Tregs to promote growth. J Clin Invest *133*. 10.1172/JCI164599.
670 21. Ahmed, A., Reinhold, C., Breunig, E., Phan, T.S., Dietrich, L., Kostadinova, F., Urwyler,
671 C., Merk, V.M., Noti, M., Toja da Silva, I., et al. (2023). Immune escape of colorectal
672 tumours via local LRH-1/Cyp11b1-mediated synthesis of immunosuppressive
673 glucocorticoids. Mol Oncol *17*, 1545-1566. 10.1002/1878-0261.13414.

674 22. Michalek, S., Goj, T., Plazzo, A.P., Marovca, B., Bornhauser, B., and Brunner, T. (2022).
675 LRH-1/NR5A2 interacts with the glucocorticoid receptor to regulate glucocorticoid
676 resistance. EMBO Rep *23*, e54195. 10.15252/embr.202154195.
677 23. Merk, V.M., Grob, L., Fleischmann, A., and Brunner, T. (2023). Human lung carcinomas
678 synthesize immunoregulatory glucocorticoids. Genes Immun *24*, 52-56.
679 10.1038/s41435-023-00194-y.
680 24. Sidler, D., Renzulli, P., Schnoz, C., Berger, B., Schneider-Jakob, S., Fluck, C., Inderbitzin,
681 D., Corazza, N., Candinas, D., and Brunner, T. (2011). Colon cancer cells produce
682 immunoregulatory glucocorticoids. Oncogene *30*, 2411-2419. 10.1038/onc.2010.629.
683 25. Pramanik, J., Shaji, S.K., Zaman, M., Brown, B., Zhang, B., Yamashita-Kanemaru, Y.,
684 Homer, N.Z.M., Hussein, H., Zhao, Q., Okkenhaug, K., et al. (2025). Drug repurposing
685 reveals Posaconazole as a CYP11A1 inhibitor enhancing anti-tumour immunity.
686 bioRxiv, 2025.2002.2021.639414. 10.1101/2025.02.21.639414.
687 26. Kurten, C.H.L., Kulkarni, A., Cillo, A.R., Santos, P.M., Roble, A.K., Onkar, S., Reeder, C.,
688 Lang, S., Chen, X., Duvvuri, U., et al. (2021). Investigating immune and non-immune
689 cell interactions in head and neck tumors by single-cell RNA sequencing. Nat Commun
690 *12*, 7338. 10.1038/s41467-021-27619-4.
691 27. Janjic, B.M., Kulkarni, A., Ferris, R.L., Vujanovic, L., and Vujanovic, N.L. (2022). Human
692 B Cells Mediate Innate Anti-Cancer Cytotoxicity Through Concurrent Engagement of
693 Multiple TNF Superfamily Ligands. Front Immunol *13*, 837842.
694 10.3389/fimmu.2022.837842.
695 28. Wang, J., Li, H., Kulkarni, A., Anderson, J.L., Upadhyay, P., Onyekachi, O.V., Arantes, L.,
696 Banerjee, H., Kane, L.P., Zhang, X., et al. (2025). Differential impact of TIM-3 ligands
697 on NK cell function. J Immunother Cancer *13*. 10.1136/jitc-2024-010618.
698 29. Pal, B., Chen, Y., Vaillant, F., Capaldo, B.D., Joyce, R., Song, X., Bryant, V.L., Penington,
699 J.S., Di Stefano, L., Tubau Ribera, N., et al. (2021). A single-cell RNA expression atlas of
700 normal, preneoplastic and tumorigenic states in the human breast. EMBO J *40*,
701 e107333. 10.15252/embj.2020107333.
702 30. Chen, Y., Pal, B., Lindeman, G.J., Visvader, J.E., and Smyth, G.K. (2022). R code and
703 downstream analysis objects for the scRNA-seq atlas of normal and tumorigenic
704 human breast tissue. Sci Data *9*, 96. 10.1038/s41597-022-01236-2.
705 31. Zilionis, R., Engblom, C., Pfirschke, C., Savova, V., Zemmour, D., Saatcioglu, H.D.,
706 Krishnan, I., Maroni, G., Meyerovitz, C.V., Kerwin, C.M., et al. (2019). Single-Cell
707 Transcriptomics of Human and Mouse Lung Cancers Reveals Conserved Myeloid
708 Populations across Individuals and Species. Immunity *50*, 1317-1334 e1310.
709 10.1016/j.immuni.2019.03.009.
710 32. Steele, N.G., Carpenter, E.S., Kemp, S.B., Sirihorachai, V.R., The, S., Delrosario, L.,
711 Lazarus, J., Amir, E.D., Gunchick, V., Espinoza, C., et al. (2020). Multimodal Mapping of
712 the Tumor and Peripheral Blood Immune Landscape in Human Pancreatic Cancer. Nat
713 Cancer *1*, 1097-1112. 10.1038/s43018-020-00121-4.
714 33. Halbrook, C.J., Thurston, G., Boyer, S., Anaraki, C., Jimenez, J.A., McCarthy, A., Steele,
715 N.G., Kerk, S.A., Hong, H.S., Lin, L., et al. (2022). Differential integrated stress response
716 and asparagine production drive symbiosis and therapy resistance of pancreatic
717 adenocarcinoma cells. Nat Cancer *3*, 1386-1403. 10.1038/s43018-022-00463-1.
718

Figure legends

Figure 1. Genome-wide effect of glucocorticoid signalling in activated CD8 T cell

- **a.** Schematic flowchart of the experimental strategy. CD8 T cells from three healthy donors were purified, activated and propagated. Resting T cells were reactivated the presence or absence of physiological level (100 nM) cortisol to find out glucocorticoid-regulated genes in CD8 T cells by RNA-seq.
  Specification of the samples (b-g): KO denotes GR knockout, Mock denotes wildtype, HC denotes hydrocortisone (cortisol) treated. Veh denotes vehicle.
- **b.** Volcano plot depicting the differentially expressed genes in human primary activated CD8 T cells after cortisol treatment. The significantly upregulated genes have been shown in red and the significantly downregulated genes have been shown in blue. log2-Fold change versus –log10(adjusted p-value) has been plotted, n = 3 human samples in each group.
- **c.** The hallmark biological processes associated with cortisol-treated CD8 T cells. Prognosis-ranked gene set enrichment analysis (GSEA) identified hallmark pathways that are differentially regulated. Normalised enrichment scores (NES) were calculated for all 50 hallmark pathways in GSEA. Upregulated (shown in red) and downregulated (shown in blue) gene sets are displayed, with their NES values represented on the x-axis.
- **d.** Knockout (KO) of glucocorticoid receptor encoding gene *NR3C1* in CD8 T cells using CRISPR-Cas9 targeting exon 2 and exon 5 (top panel). The knockout efficiency has been validated by western blot (bottom panel).
- **e.** Volcano plot showing the differentially expressed genes in *NR3C1* KO activated CD8 T cells compared to mock activated CD8 T cells, in the presence of cortisol.
- **f.** The intersections in Venn diagrams showing the cortisol-induced GR-dependent upregulated and downregulated genes.
- **g.** Expression heatmap showing the cortisol-induced transcription factors and receptors (cytokine receptor, transporter type receptor, cell surface and adhesion receptor, nuclear receptor) from differentially expressed genes (log2FC> 1, log2FC <-1 and p.adj > 0.05).

Figure 2. Genome-wide chromatin binding of GR identifies non-canonical transcription factor binding motif in CD8 T cells

- **a.** Diagrammatic flowchart of the experimental strategy. CD8 T cells from healthy donors were purified, activated and propagated. Resting CD8 T cells were

reactivated the presence or absence of physiological level (100 nM) cortisol to find out genome-wide chromatin binding of GR by ChIP-seq.

b. Homer motif analysis of cortisol-treated CD8 T cells. The top 4 enriched GR binding peaks and corresponding motifs have been shown for two donors (HC-A & HC-B) in cortisol-treated CD8 T Cells. HC-A & HC-B: Hydrocortisone (HC)/cortisol-treated donor-A & donor-B samples.

c. Venn diagram showing the common number of peaks between hydrocortisone (cortisol) treated CD8 T cells from two donors ,

d. Venn diagram showing glucocorticoid (GC)-induced peaks comparing vehicle-treated and cortisol (HC)-treated CD8 T cells.

e. The Venn diagram shows the direct targets of glucocorticoids after intersecting GR binding peaks from ChIP-seq data and cortisol-induced upregulated genes.

f. The Venn diagram shows all GR-RUNX co-regulated genes that are also direct targets of GR.

g. Snapshot of glucocorticoid binding peaks around indicated representative genes from the UCSC genome browser. Glucocorticoid influenced and GR -RUNX regulated top five genes have been shown here.

h. GR-binding site frequencies representing diversity of glucocorticoid receptor binding sites in CD8 T cells.

Figure 3. RUNX transcription factors cooperate with the glucocorticoid receptor to regulate gene expression

a. Schematic illustration of the experimental strategy (left). HEK 293T cells were transfected with GR and RUNX3 expressing plasmid construct. Nuclear lysates were immunoprecipitated by using anti-GR antibody and immunoblotted by RUNX antibody. Representative immunoblot shown in the right panel.

b. Venn diagram depicting the set of genes jointly regulated by the GR and RUNX1, identified through an integrative analysis of cortisol-induced upregulated genes, GR ChIP-seq peaks, GR peaks containing RUNX1 motifs, and known RUNX1 target genes. Expression levels of the overlapping gene set are visualised in a heatmap across multiple experimental conditions.

c. Venn diagram illustrating the genes co-regulated by GR and RUNX2, identified by integrating cortisol-responsive genes (both upregulated and downregulated), GR ChIP-seq data, GR peaks with RUNX2 motifs, and annotated RUNX2 targets. Expression patterns of these shared genes under different conditions are shown in the accompanying heatmap. Specification of the samples: KO denotes glucocorticoid

receptor (GR) knockout, HC denotes hydrocortisone (cortisol) treated. Mock denotes wildtype. Veh denotes vehicle.

Figure 4. Single-cell transcriptomics study reveals the expression of cortisol responder genes in different tumour-infiltrating CD8 T cells

a-d. UMAP-based clustering of scRNA-seq data was used to identify CD8 T cell populations from tumour and matched blood or normal tissue samples in breast cancer (**a**), lung cancer (**b**), head and neck squamous cell carcinoma (HNSC) (**c**), and pancreatic ductal adenocarcinoma (PDAC) (**d**). Dot plots show the proportion of cells (dot size) and the average expression (colour intensity) of selected top cortisol responder genes, *NR3C1*, *TSC22D3*, *AREG*, *FKBP5*, and *PIK3IP1*, within tumour-infiltrating CD8 T cells and corresponding peripheral blood or matched tissue-resident CD8 T cells. The data highlight distinct patterns of steroid-responsive gene expression between tumour-infiltrating and non-tumour CD8 T cell populations, reflecting the influence of the tumour microenvironment on CD8 T cell transcriptional states and potential links to T cell dysfunction and immune evasion

Figure 5. RUNX and GR co-regulated gene expression in tumour-infiltrating CD8 T cells across cancer types

a-d. Single-cell transcriptomic profiling was performed on CD8 T cells isolated from tumours and matched adjacent normal tissue or blood in triple-negative breast cancer (TNBC) (**a**), lung cancer (**b**), head and neck squamous cell carcinoma (HNSC) (**c**), and pancreatic ductal adenocarcinoma (PDAC) (**d**). UMAP-based clustering delineated distinct CD8 T cell populations. Dot plots display both the proportion of cells (dot size) and the average expression (colour intensity) of RUNX (RUNX1, 2 and 3) and GR co-regulated genes within tumour-infiltrating and peripheral or tissue-resident CD8 T cells. This analysis reveals elevated expression of RUNX and GR combined target genes in tumour-infiltrating CD8 T cells compared to their non-tumour counterparts, suggesting a tumour microenvironment-driven transcriptional programme.

e-h. To assess the functional relevance of RUNX and GR co-regulated gene expression, module scores were calculated using the AddModuleScore method for each CD8 T cell. High module scores, indicative of elevated co-regulated gene expression, were associated with increased expression of exhaustion-related genes, highlighting a link between RUNX2/GR transcriptional activity and the exhausted phenotype in tumour-infiltrating CD8 T cells across TNBC **(e)**, lung cancer **(f)**, HNSC **(g)**, and PDAC **(h)**.

Supplementary Figure S1. Comparative *RUNX 1, 2* and *3* expression and identification of GR-RUNX 3 co-regulated genes

- **a.** Comparative *RUNX 1, 2* and *3* expression in activated CD8 T cells in the RNAseq. Normalised expression of these genes from different donors has been plotted here.
- **b.** Venn diagrams showing the GR-RUNX3 co-regulated genes by integrating cortisol induced genes (upregulated and downregulated), all GR binding peaks from ChIP-seq, GR binding site containing RUNX motif and RUNX3 target genes. The corresponding heatmap showing the expression of GR-RUNX3 co-regulated genes in vehicle-treated CD8 T cells, cortisol (hydrocortisone or HC) treated CD8 T cell and *NR3C1* KO CD8 T cells.

Supplementary Figure S2. Single-cell trajectory analysis of CD8 T cells from lung tumours and blood samples

- **a.** Pseudo-temporal trajectories of CD8 T cells inferred using Monocle, coloured by sample origin and pseudotime.
- **b.** Expression patterns of cortisol-responsive genes (*TSC22D3, IL7R, FKBP5*) and inhibitory receptors (*PDCD1, CTLA4, HAVCR2, TIGIT, LAYN, TOX*) along the inferred trajectories.

Figure 1

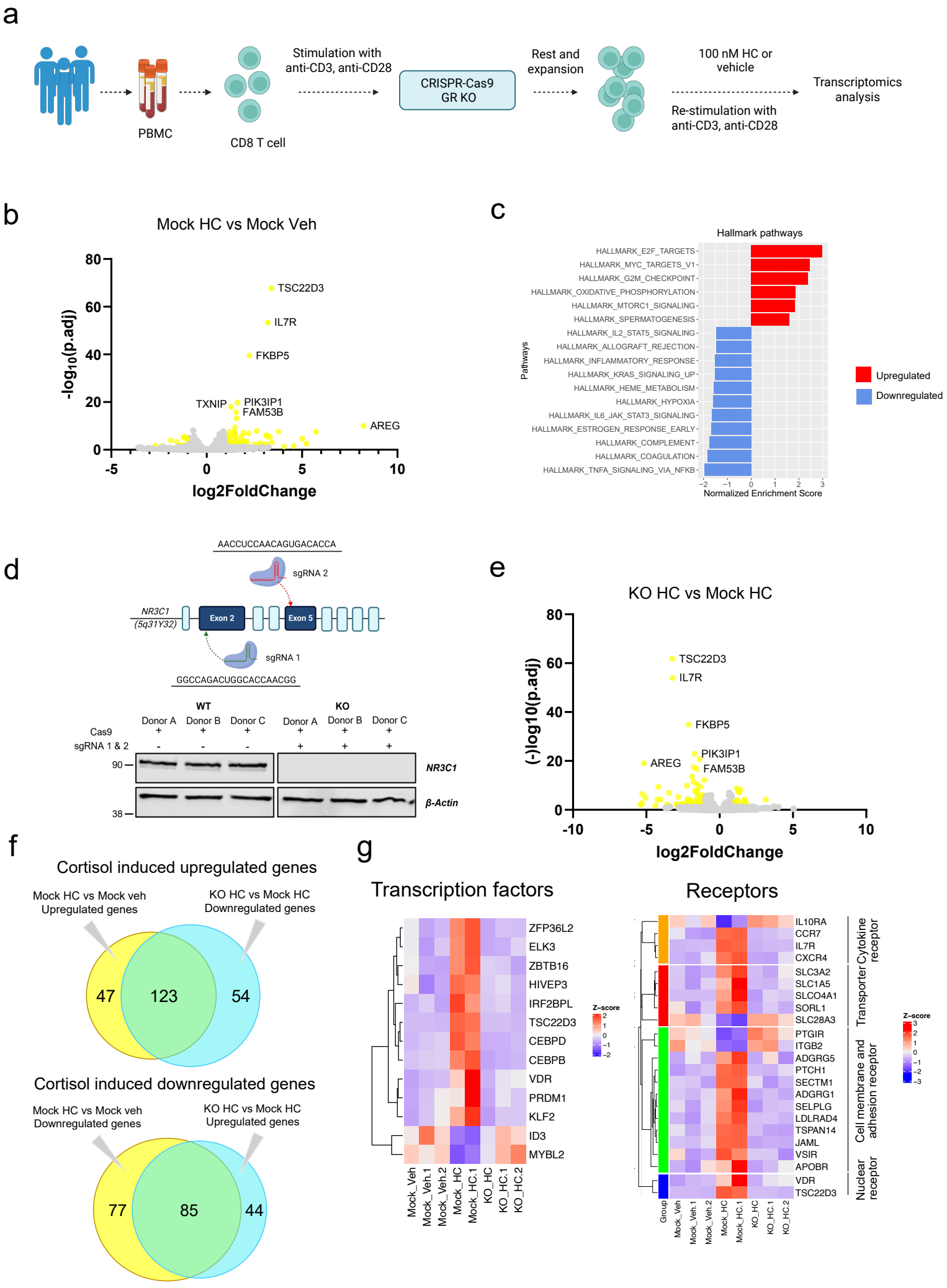
a
PBMC
CD8 T cell
Stimulation with anti-CD3, anti-CD28
CRISPR-Cas9 GR KO
Rest and expansion
100 nM HC or vehicle
Re-stimulation with anti-CD3, anti-CD28
Transcriptomics analysis
b
Mock HC vs Mock Veh
-log10(p.adj)
log2FoldChange
TSC22D3
IL7R
FKBP5
TXNIP
PIK3IP1
FAM53B
AREG
c
Hallmark pathways
Pathways
Normalized Enrichment Score
HALLMARK_E2F_TARGETS
HALLMARK_MYC_TARGETS_V1
HALLMARK_G2M_CHECKPOINT
HALLMARK_OXIDATIVE_PHOSPHORYLATION
HALLMARK_MTORC1_SIGNALING
HALLMARK_SPERMATOGENESIS
HALLMARK_IL2_STAT5_SIGNALING
HALLMARK_ALLOGRAFT_REJECTION
HALLMARK_INFLAMMATORY_RESPONSE
HALLMARK_KRAS_SIGNALING_UP
HALLMARK_HEME_METABOLISM
HALLMARK_HYPOXIA
HALLMARK_IL6_JAK_STAT3_SIGNALING
HALLMARK_ESTROGEN_RESPONSE_EARLY
HALLMARK_COMPLEMENT
HALLMARK_COAGULATION
HALLMARK_TNFA_SIGNALING_VIA_NFKB
Upregulated
Downregulated
d
AACCUCCAACAGUGACACCA
sgRNA 2
NR3C1 (5q31Y32)
Exon 2
Exon 5
sgRNA 1
GGCCAGACUGGCACCAACGG
WT
KO
Donor A
Donor B
Donor C
Cas9
sgRNA 1 & 2
NR3C1
β-Actin
e
KO HC vs Mock HC
(-)log10(p.adj)
log2FoldChange
TSC22D3
IL7R
FKBP5
PIK3IP1
FAM53B
AREG
f
Cortisol induced upregulated genes
Mock HC vs Mock veh Upregulated genes
KO HC vs Mock HC Downregulated genes
47
123
54
Cortisol induced downregulated genes
Mock HC vs Mock veh Downregulated genes
KO HC vs Mock HC Upregulated genes
77
85
44
g
Transcription factors
ZFP36L2
ELK3
ZBTB16
HIVEP3
IRF2BPL
TSC22D3
CEBPD
CEBPB
VDR
PRDM1
KLF2
ID3
MYBL2
Z-score
Mock_Veh
Mock_Veh.1
Mock_Veh.2
Mock_HC
Mock_HC.1
KO_HC
KO_HC.1
KO_HC.2
Receptors
IL10RA
CCR7
IL7R
CXCR4
SLC3A2
SLC1A5
SLCO4A1
SORL1
SLC28A3
PTGIR
ITGB2
ADGRG5
PTCH1
SECTM1
ADGRG1
SELPLG
LDLRAD4
TSPAN14
JAML
VSIR
APOBR
VDR
TSC22D3
Cytokine receptor
Transporter
Cell membrane and adhesion receptor
Nuclear receptor
Group

Figure 2

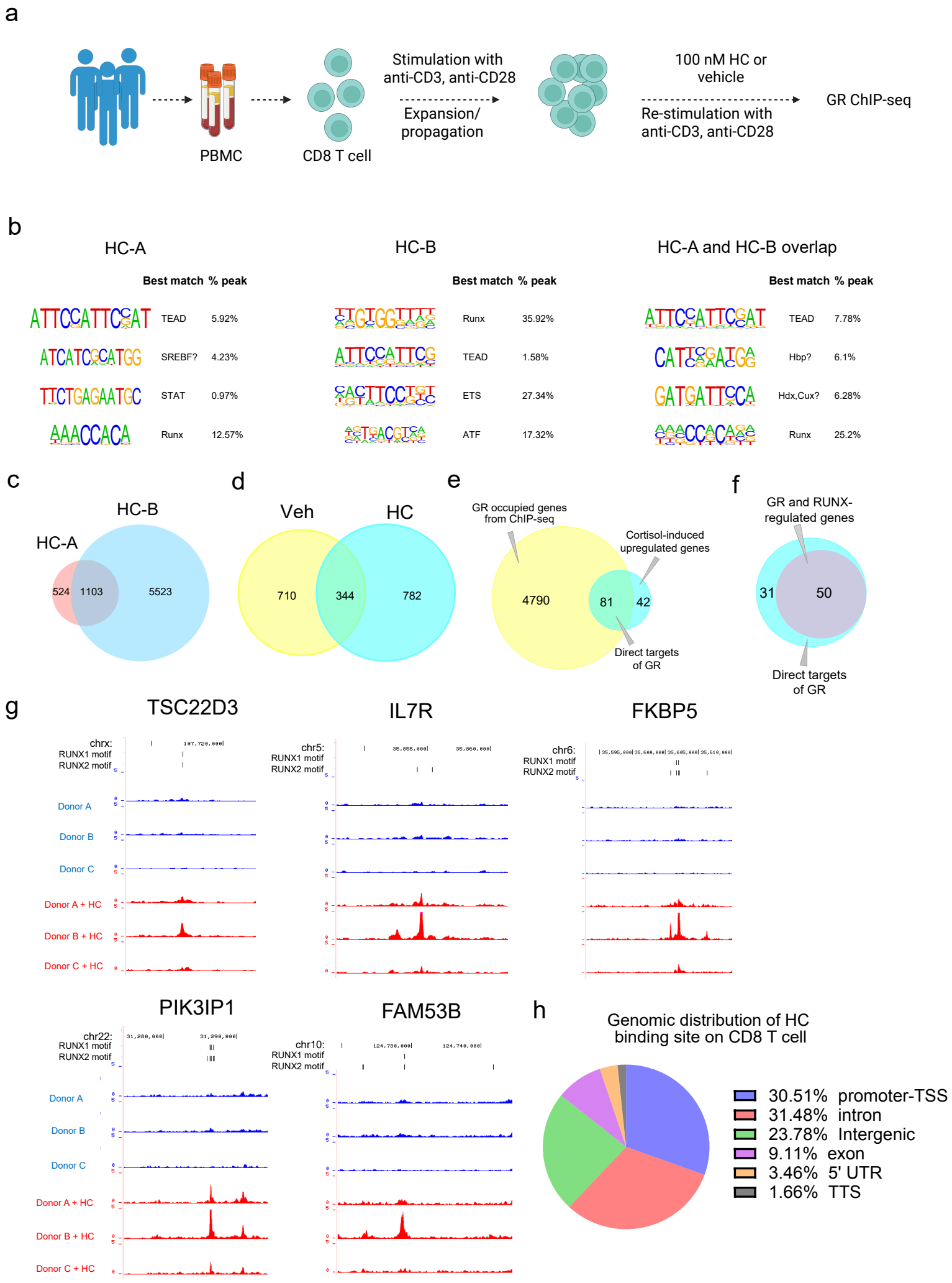
a
PBMC
CD8 T cell
Stimulation with anti-CD3, anti-CD28
Expansion/ propagation
100 nM HC or vehicle
Re-stimulation with anti-CD3, anti-CD28
GR ChIP-seq
b
HC-A
Best match % peak
TEAD 5.92%
SREBF? 4.23%
STAT 0.97%
Runx 12.57%
HC-B
Best match % peak
Runx 35.92%
TEAD 1.58%
ETS 27.34%
ATF 17.32%
HC-A and HC-B overlap
Best match % peak
TEAD 7.78%
Hbp? 6.1%
Hdx,Cux? 6.28%
Runx 25.2%
c
HC-A
HC-B
524
1103
5523
d
Veh
HC
710
344
782
e
GR occupied genes from ChIP-seq
Cortisol-induced upregulated genes
4790
81
42
Direct targets of GR
f
GR and RUNX-regulated genes
31
50
Direct targets of GR
g
TSC22D3
IL7R
FKBP5
chrx:
chr5:
chr6:
RUNX1 motif
RUNX2 motif
Donor A
Donor B
Donor C
Donor A + HC
Donor B + HC
Donor C + HC
PIK3IP1
FAM53B
chr22:
chr10:
h
Genomic distribution of HC binding site on CD8 T cell
30.51% promoter-TSS
31.48% intron
23.78% Intergenic
9.11% exon
3.46% 5' UTR
1.66% TTS

Figure 3

a

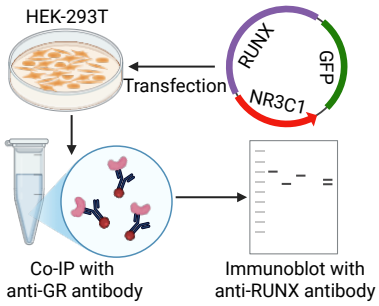
HEK-293T
Transfection
RUNX
GFP
NR3C1
Co-IP with
anti-GR antibody
Immunoblot with
anti-RUNX antibody

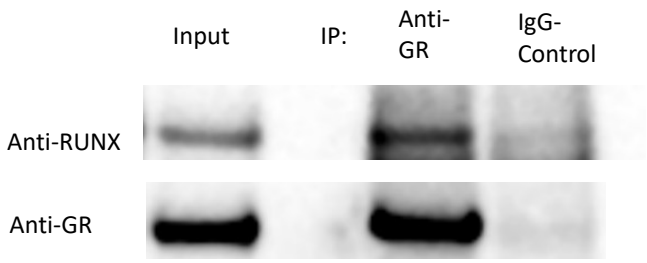
Input
IP:
Anti-GR
IgG-Control
Anti-RUNX
Anti-GR

b

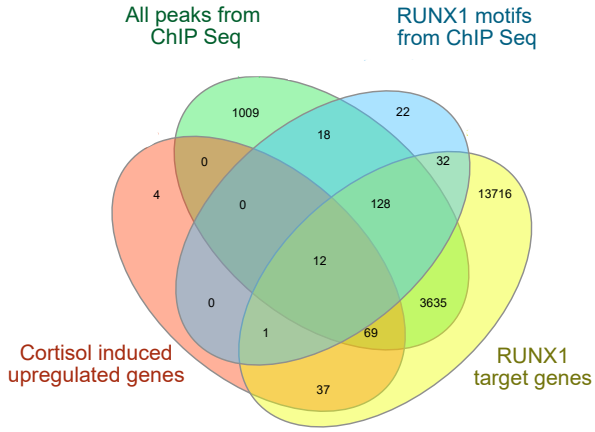
All peaks from
ChIP Seq
RUNX1 motifs
from ChIP Seq
Cortisol induced
upregulated genes
RUNX1
target genes
1009
22
18
0
32
4
0
128
13716
12
0
3635
1
69
37

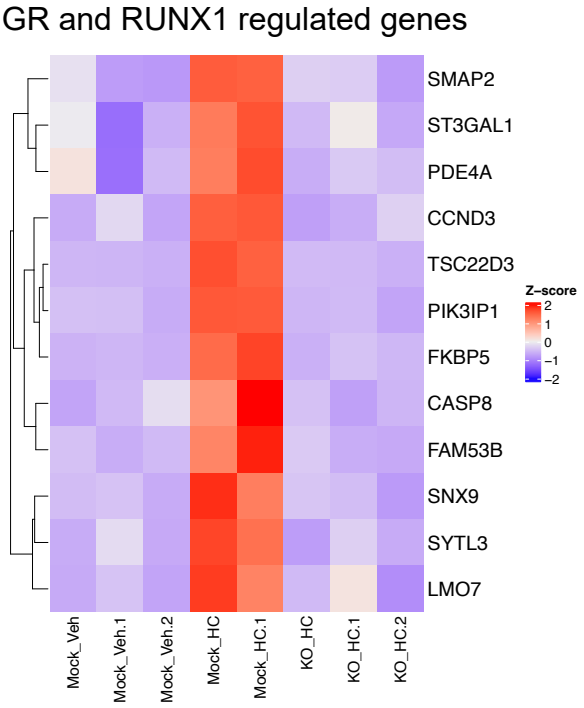
GR and RUNX1 regulated genes
SMAP2
ST3GAL1
PDE4A
CCND3
TSC22D3
PIK3IP1
FKBP5
CASP8
FAM53B
SNX9
SYTL3
LMO7
Z-score
2
1
0
−1
−2
Mock_Veh
Mock_Veh.1
Mock_Veh.2
Mock_HC
Mock_HC.1
KO_HC
KO_HC.1
KO_HC.2

c

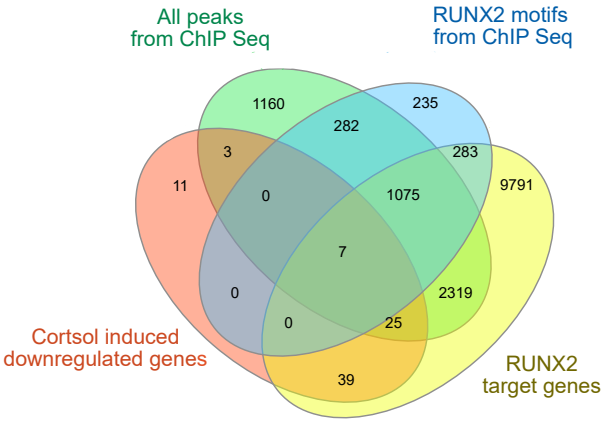
All peaks
from ChIP Seq
RUNX2 motifs
from ChIP Seq
Cortsol induced
downregulated genes
RUNX2
target genes
1160
235
282
3
283
11
0
1075
9791
7
0
2319
0
25
39

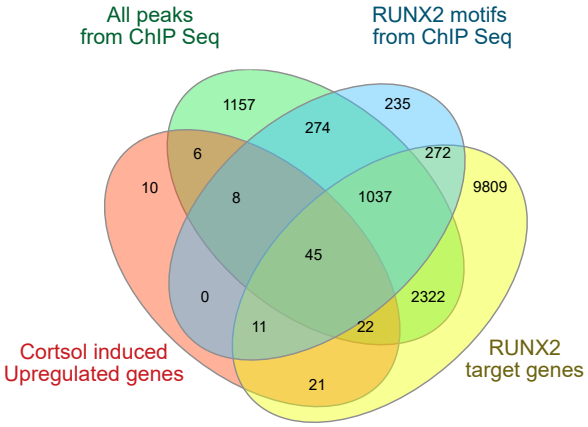
All peaks
from ChIP Seq
RUNX2 motifs
from ChIP Seq
Cortsol induced
Upregulated genes
RUNX2
target genes
1157
235
274
6
272
10
8
1037
9809
45
0
2322
11
22
21

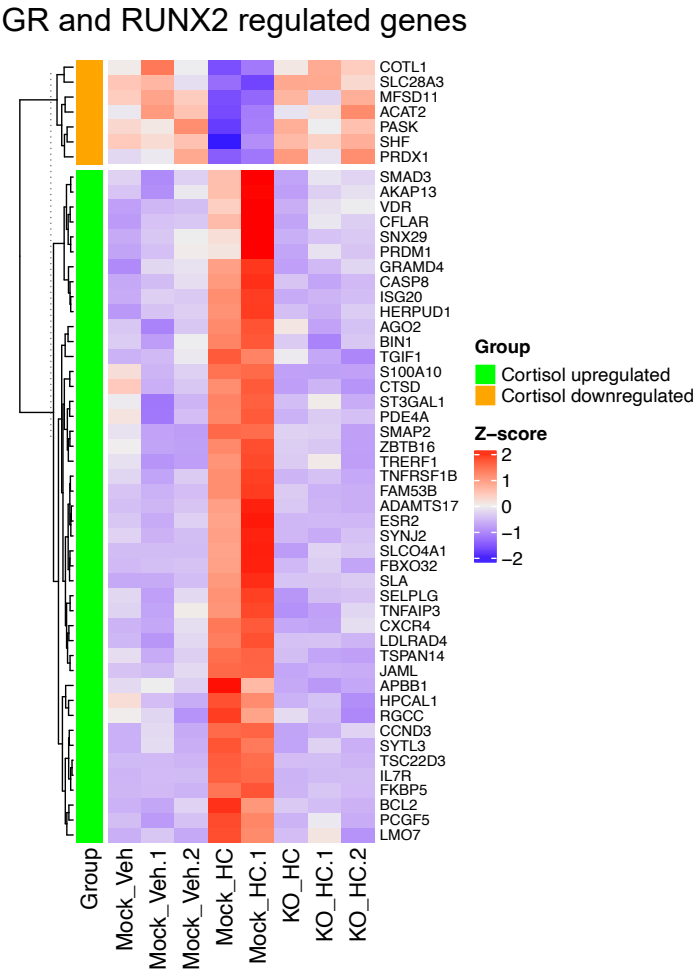
GR and RUNX2 regulated genes
COTL1
SLC28A3
MFSD11
ACAT2
PASK
SHF
PRDX1
SMAD3
AKAP13
VDR
CFLAR
SNX29
PRDM1
GRAMD4
CASP8
ISG20
HERPUD1
AGO2
BIN1
TGIF1
S100A10
CTSD
ST3GAL1
PDE4A
SMAP2
ZBTB16
TRERF1
TNFRSF1B
FAM53B
ADAMTS17
ESR2
SYNJ2
SLCO4A1
FBXO32
SLA
SELPLG
TNFAIP3
CXCR4
LDLRAD4
TSPAN14
JAML
APBB1
HPCAL1
RGCC
CCND3
SYTL3
TSC22D3
IL7R
FKBP5
BCL2
PCGF5
LMO7
Group
Cortisol upregulated
Cortisol downregulated
Z-score
2
1
0
−1
−2
Group
Mock_Veh
Mock_Veh.1
Mock_Veh.2
Mock_HC
Mock_HC.1
KO_HC
KO_HC.1
KO_HC.2

Figure 4

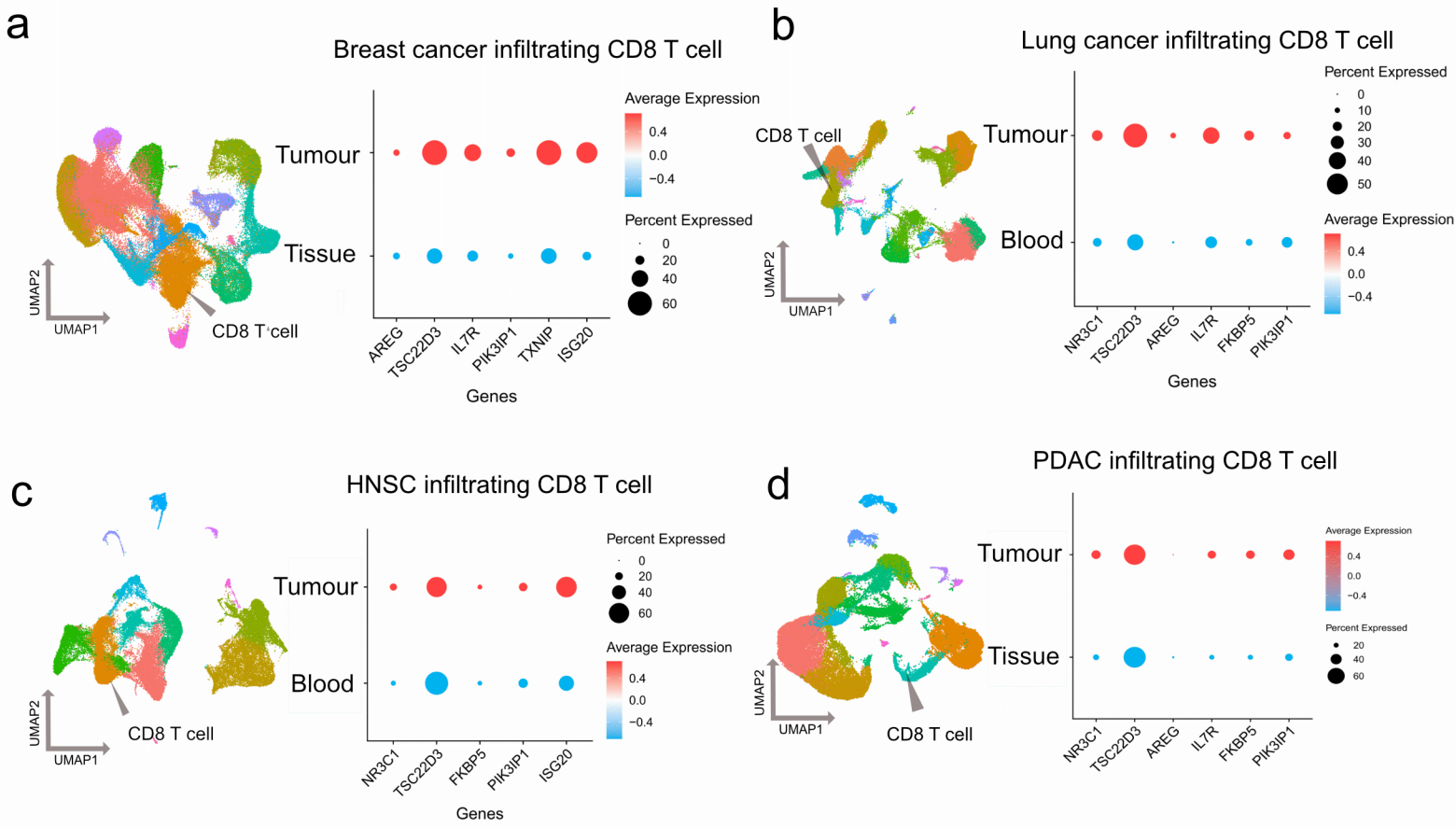
a
Breast cancer infiltrating CD8 T cell
Tumour
Tissue
CD8 T cell
UMAP2
UMAP1
AREG
TSC22D3
IL7R
PIK3IP1
TXNIP
ISG20
Genes
Average Expression
0.4
0.0
−0.4
Percent Expressed
0
20
40
60
b
Lung cancer infiltrating CD8 T cell
CD8 T cell
Tumour
Blood
UMAP2
UMAP1
NR3C1
TSC22D3
AREG
IL7R
FKBP5
PIK3IP1
Genes
Percent Expressed
0
10
20
30
40
50
Average Expression
0.4
0.0
−0.4
c
HNSC infiltrating CD8 T cell
Tumour
Blood
CD8 T cell
UMAP2
UMAP1
NR3C1
TSC22D3
FKBP5
PIK3IP1
ISG20
Genes
Percent Expressed
0
20
40
60
Average Expression
0.4
0.0
−0.4
d
PDAC infiltrating CD8 T cell
Tumour
Tissue
CD8 T cell
UMAP2
UMAP1
NR3C1
TSC22D3
AREG
IL7R
FKBP5
PIK3IP1
Average Expression
0.4
0.0
−0.4
Percent Expressed
20
40
60

Figure 5

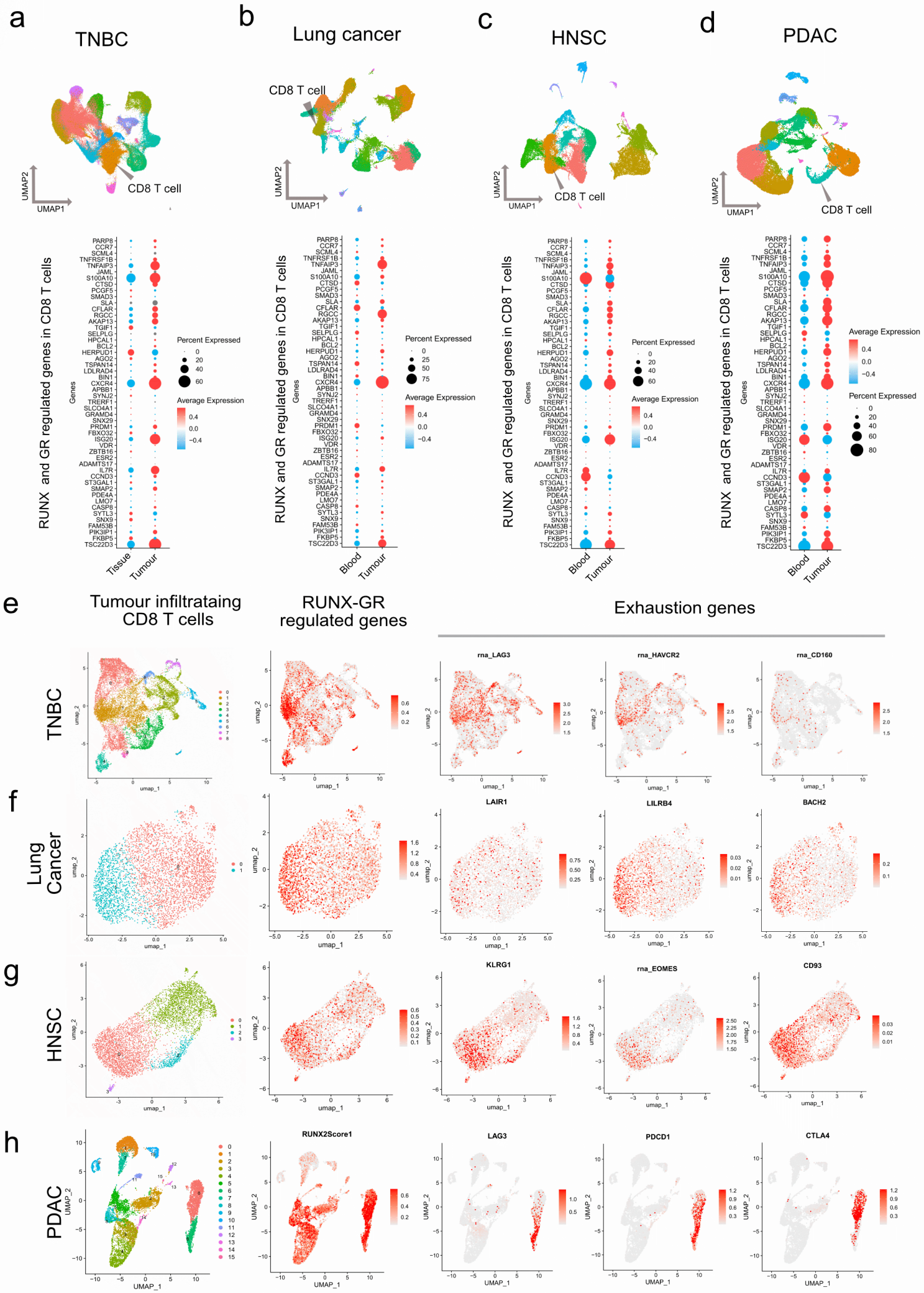
a
TNBC
CD8 T cell
UMAP2
UMAP1
b
Lung cancer
CD8 T cell
c
HNSC
CD8 T cell
d
PDAC
CD8 T cell
RUNX and GR regulated genes in CD8 T cells
Genes
Percent Expressed
Average Expression
Tissue
Tumour
Blood
e
Tumour infiltrataing CD8 T cells
RUNX-GR regulated genes
Exhaustion genes
TNBC
rna_LAG3
rna_HAVCR2
rna_CD160
f
Lung Cancer
LAIR1
LILRB4
BACH2
g
HNSC
KLRG1
rna_EOMES
CD93
h
PDAC
RUNX2Score1
LAG3
PDCD1
CTLA4
umap_1
umap_2
UMAP_1
UMAP_2

Supplementary Figure S1

a

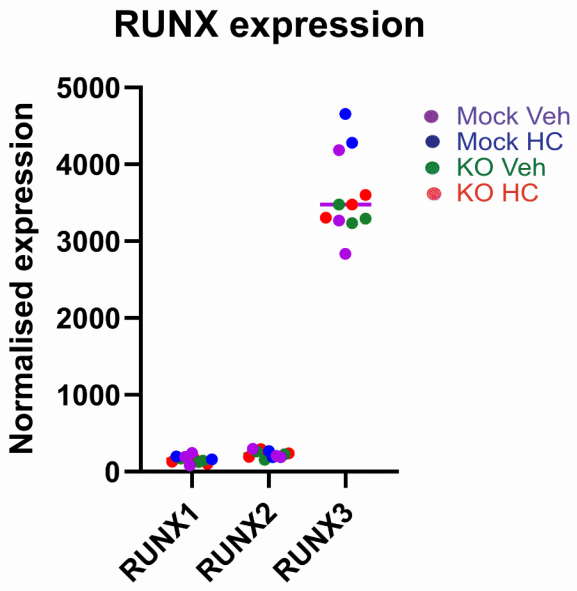

b

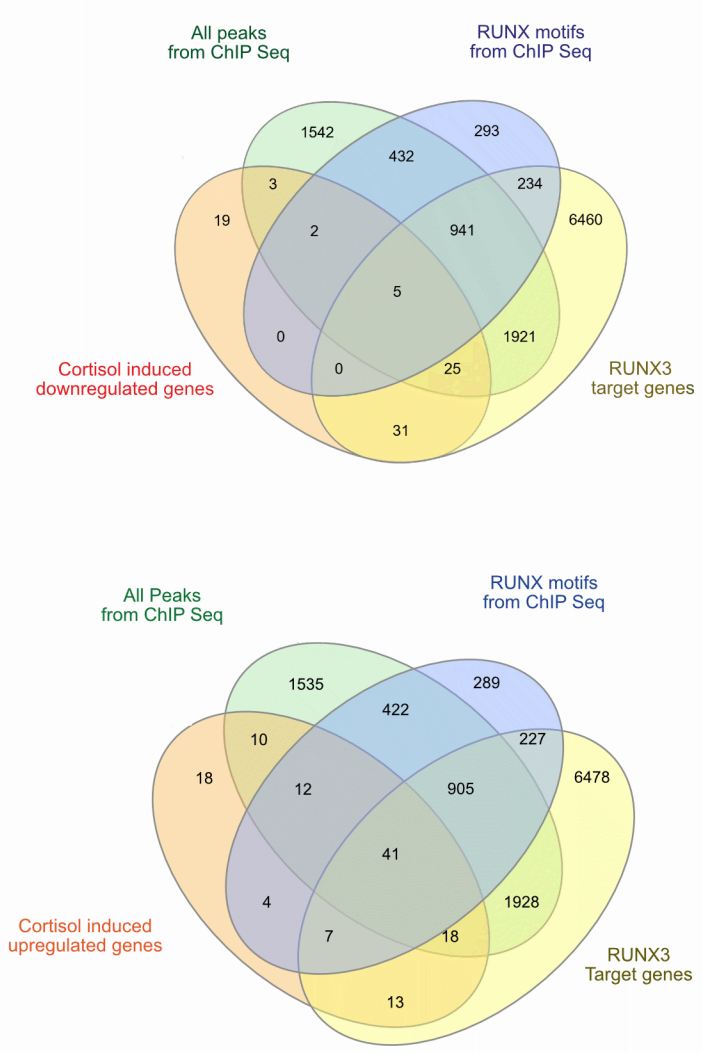

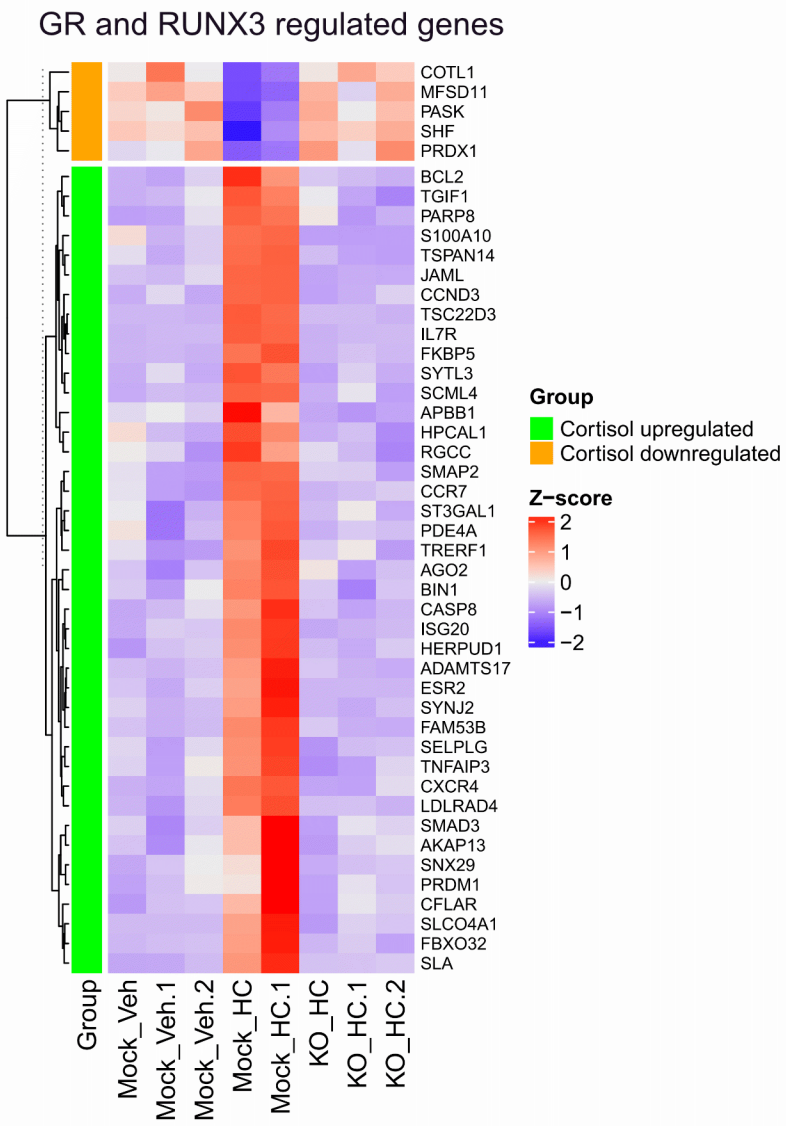

Supplementary Figure S2

a

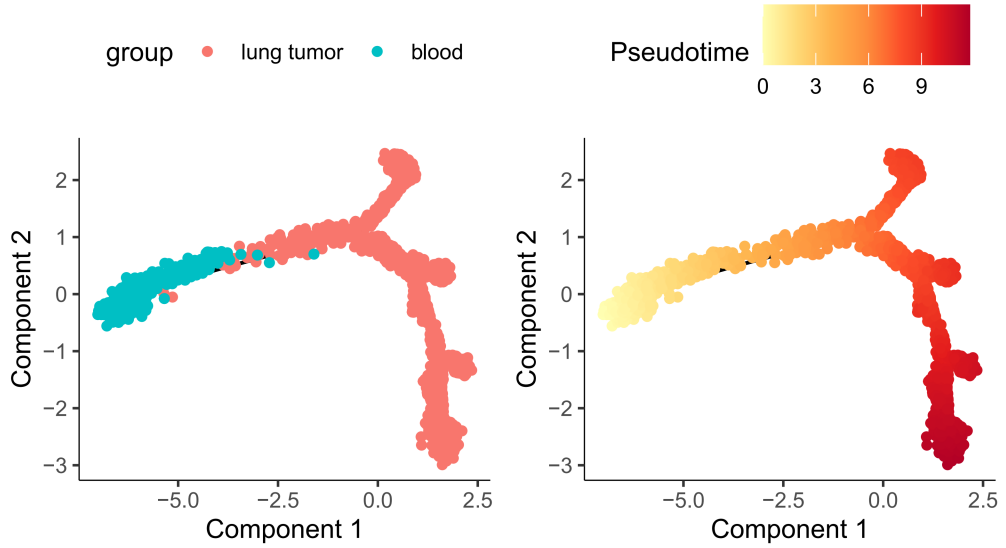
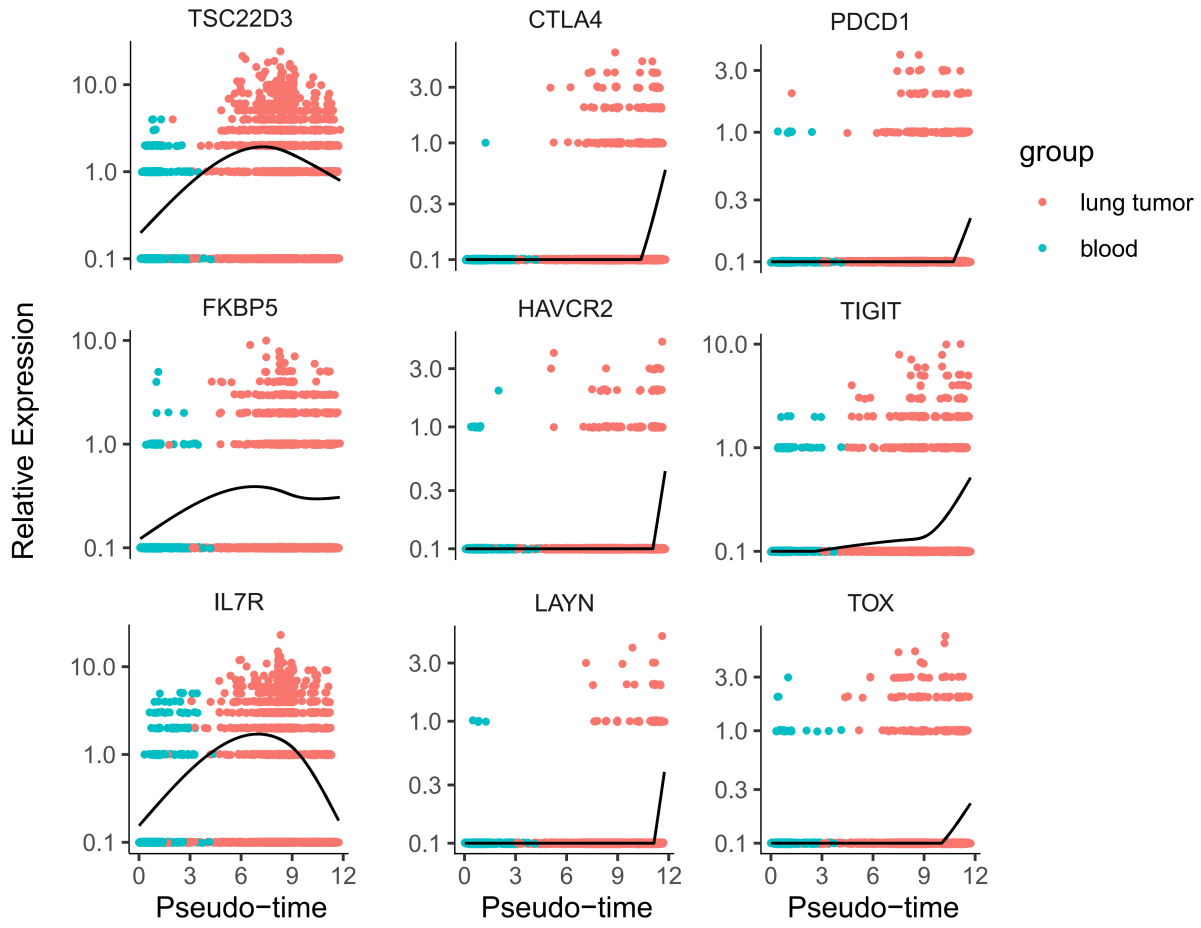
b